SSRG International Journal of Mechanical Engineering
ISSN: 2348-8360/ https://doi.org/10.14445/23488360/IJME-V13I9P101

Volume 13 Issue 9, 1-19, September 2026

Original Article

Thermal Error Prediction of a Three-Axis CNC Machine Tool using an Artificial Neural Network with Optimized Hidden-Neuron Architecture

Nguyen Trong Minh[1], Dang Duc Thuan[2]

[1]*Faculty of Engineering, Vietnam National University of Agriculture, Hanoi 12428, Vietnam.*
[2]*Mechanical Power Engineering and Automation research group, University of Transport Technology, Hanoi 100000, Vietnam.*

[1]*Corresponding Author : ntminh@vnua.edu.vn*

Received: 25 June 2026 Revised: 05 August 2026 Accepted: 21 August 2026 Published: 26 September 2026

Abstract *- Thermal errors are one of the major factors that affect the positioning accuracy of CNC machine tools and hence the quality of the manufactured products. Artificial Neural Networks (ANNs) have been extensively used for modeling the thermal errors, but the impact of hidden-layer architecture on the prediction accuracy remains insufficiently explored. In this study, a Neuron-Optimized Artificial Neural Network (NO-ANN) model is proposed for predicting the thermal positioning errors of a three-axis CNC machine tool. The effect of the hidden-layer neuron configuration was systematically examined to determine the optimal configuration to capture the nonlinear relationship between the thermal variations and positioning errors. The model performance was assessed by Coefficient of Determination (R^2), Root Mean Square Error (RMSE), and Mean Absolute Error (MAE). The optimized architecture of 11 hidden neurons demonstrated the highest overall performance, with an R^2 value of 0.998, RMSE of 1.3247 μm, and MAE of 0.6539 μm, and the model showed high accuracy in both training and testing sets, indicating its robustness and generalization ability. Compared with previously reported thermal error prediction models, the proposed NO-ANN achieved comparable or superior predictive accuracy while requiring only 11 hidden neurons, indicating reduced model complexity and improved computational efficiency. The results indicate that the systematic optimization of hidden-layer neurons can significantly improve the accuracy of thermal error prediction of ANNs, which can be used to effectively compensate for the thermal error in intelligent CNC machining systems.*

Keywords *- Artificial Neural Network, CNC machine tool, Hidden neuron optimization, Machining precision, Thermal error prediction.*

1. Introduction

Computer Numerical Control (CNC) machine tools are designed to perform complex machining operations, such as cutting, turning, milling, and drilling, with high precision through advanced numerical control systems. The positioning accuracy of CNC machine tools is influenced by multiple factors, including structural inaccuracies, cutting-tool condition, and the performance of the machine control system [1, 2]. Among these, geometric and thermal-induced errors together account for approximately 70% of the total volumetric error observed in machine tools [3]. Nevertheless, thermal errors remain one of the primary sources of machining inaccuracies. Thermal errors are dimensional, geometric or positional errors which are produced by the temperature change of the machine tool system [4-8]. Industries such as the aerospace, automotive and medical manufacturing sectors require CNC machine tools to perform with micrometer precision, which is what modern machines do. Temperature variations can cause thermal deformation of critical machine components, including the machine frame, spindle, and worktable, thereby altering the relative position between the cutting tool and the workpiece [9-12]. Therefore, thermal error is one of the most serious problems to be overcome in order to obtain and maintain high machining accuracy.

Thermal errors in machine tools are caused by both internal and external heat sources, and are considered to be one of the most important factors that influence the accuracy of CNC machining systems [7, 13, 14]. Beyond temperature variation alone, recent studies have shown that thermal errors are also influenced by additional factors such as heat-source distribution and energy consumption, which are frequently overlooked in conventional thermal error models [15]. In general, the internal heat generation is the most important source of thermal deformation [16]. These heat sources are from the normal running process of the machine tool. There is significant heat generated in moving parts such as bearings, spindles and feed drive mechanisms. For example, when the spindle rotates at high speeds, it can be several thousand revolutions per minute, which produces localized increases in temperature due to friction. Furthermore, servo motors and stepper motors, which drive the X-, Y-, and Z-axes continuously generate heat during operation, especially when the machines are in use for extended periods of time. Further, a considerable amount of thermal energy is generated during the material removal process, as a result of friction and plastic deformation at the tool-workpiece interface. The heat generated can be conducted to the other parts of the machine, leading to non-uniform thermal expansion and geometric deviations. These heat sources are inherently related to machine tool operation and are hard to remove completely, and the effects build up during extended machining operations. Thermal error formation is also caused by external thermal sources in addition to the internal heat generation [17-19]. These sources are related to the manufacturing environment and include changes in workshop temperature, diurnal temperature fluctuations, and seasonal changes in ambient conditions. The effect of external thermal disturbances can be reduced by taking steps to control the environment, such as using air-conditioned workshops and protecting from direct sunlight, but it is still difficult to obtain complete thermal stability under practical industrial conditions.

Several methods have been proposed to reduce thermal errors of CNC machine tools. Cutting fluids are used in cooling systems to remove heat produced during machining processes and to control the temperature of critical parts, such as the spindle [18, 20]. To minimize thermally induced deformation, machine structures are also usually made from materials with low coefficients of thermal expansion, such as gray cast iron and special alloys. Thermal stability is also achieved by operating machine tools in temperature-controlled facilities (environmental control measures). Despite their effectiveness, these approaches suffer from several practical limitations. Cooling systems add to operating and maintenance expenses, and in large-scale manufacturing settings, it may be impossible to maintain strict environmental control. Therefore, numerical thermal error compensation has become an interesting solution to enhance the machining accuracy [21-25]. Thermal error compensation is a method of correcting positioning errors caused by temperature changes by moving the machine axis positions to compensate for the error that is predicted at a certain operating condition and position. Compensation-based approaches have a number of benefits over structural modification [12, 26-28]. First, they are typically cheaper than redesigning parts of the machine or adding significant thermal control measures [29]. Secondly, they are more adaptable in that they can cope with changes in the thermal error sources that cannot be adequately solved by structural changes. The performance of thermal error compensation is mainly based on the accuracy and robustness of the thermal error prediction model. Therefore, establishing reliable relationships between temperature variations and thermally induced machine tool deformation has become a major focus of thermal error research. Thermal error prediction methods can be broadly divided into three types: physics-based, statistical, and Artificial Intelligence (AI) based.

Physics-based methods, such as Finite Element Analysis (FEA), thermal network models and thermo-mechanical coupled models, model thermal deformation based on the principles of heat transfer and structural mechanics [30-32]. To overcome these limitations, statistical methods like Multiple Linear Regression (MLR), Principal Component Regression (PCR) and Partial Least Squares (PLS) regression have been developed to model the relationship between temperature variations and thermal errors [33-35]. These techniques are easy to use and simple to apply, but the complex, non-linear relationships of thermal deformation are not well described, which may result in inaccuracies in prediction under practical machining conditions. Due to the rapid progress of artificial intelligence and machine learning techniques, data-driven approaches are gaining importance in the field of thermal error prediction and compensation. Artificial Neural Networks (ANNs), Support Vector Regression (SVR), Random Forests (RF), Extreme Learning Machines (ELM), and deep learning models have been shown to have good performance in modeling the nonlinear relationship between thermal variables and thermal errors [36-39]. Among these methods, the use of ANNs has been the most popular, due to its nonlinear approximation capabilities, adaptive learning capability and immunity to measurement noise.

Although ANN-based models have demonstrated considerable capability for thermal error prediction, their predictive performance remains highly dependent on network architecture, particularly the number of hidden-layer neurons [40]. Even recent studies continue to focus predominantly on optimizing input-side factors, such as temperature-sensitive point screening [41]. Most previous studies have selected the hidden-layer size using empirical rules or trial-and-error procedures, which may lead to underfitting, overfitting, or unnecessarily complex models. Furthermore, limited attention has been devoted to evaluating the robustness of ANN architectures under different random weight initializations and stochastic training-testing partitions. Consequently, a systematic framework that jointly considers prediction accuracy, goodness-of-fit, and model robustness for hidden-layer optimization remains insufficiently explored. Accordingly, an important question remains regarding how the optimal hidden-layer architecture can be determined objectively to improve the reliability of ANN-based thermal error prediction, while maintaining both predictive accuracy and stability under stochastic training conditions. To address this issue, the present study proposes a Monte Carlo-based hidden-neuron optimization framework coupled with a composite performance score. This framework simultaneously evaluates prediction accuracy, goodness-of-fit, and model stability, thereby providing a systematic and quantitative basis for selecting an appropriate ANN architecture for thermal error prediction in three-axis CNC machine tools. The specific contributions of this study, which distinguish it from previous studies relying primarily on the Universal Approximation Theorem, are threefold. First, the number of hidden neurons is swept exhaustively over a wide range (1-30), and each configuration is evaluated over 500 Monte Carlo repetitions with independent random training-testing partitions, which removes the dependence of the reported accuracy on a single, possibly favorable, weight initialization or data split. Second, a composite performance score is proposed that simultaneously combines predictive accuracy (RMSE), Coefficient of Determination (R^2) and stability (the interquartile range of RMSE across the Monte Carlo runs) into a single, min-max normalized index, enabling an objective and reproducible criterion for architecture selection instead of the single-metric comparisons commonly used in prior ANN-based thermal error studies. Third, the convergence of this composite index is explicitly verified, providing statistical evidence that the reported optimum is stable rather than an artifact of a particular run. Taken together, these elements constitute a general, transferable methodology for hidden-layer sizing in thermal error modeling, rather than a single case-specific ANN application.

2. Materials and Methods

2.1. Experimental Data Source

The experimental data were acquired using a three-axis vertical CNC machining center with a Siemens 810D numerical control system. The machine has a travel range of 560 mm, 406 mm, and 508 mm in the X, Y, and Z directions, respectively. The spindle speed can reach 7500 rpm, and the machine has a worktable of 840 mm × 360 mm. The total installed power of the machine is 20 kVA [21, 42, 43], and the spindle is driven by a 15 kW AC motor.

Six PT100 Resistance Temperature Detectors (RTDs) were installed at representative thermal hotspots within the CNC machine to measure the temperature. Thermal sensitive areas were detected with thermographic inspection before installation of the sensors, to establish the main heat sources and heat-affected components. Two RTD sensors were placed on each machine axis (X, Y and Z) and near critical bearing and drive-system locations to monitor thermal variations during machine operation, as shown in Figure 1 [42]. The six temperature measurements were denoted as T1-T6 and continuously recorded throughout the experiments.

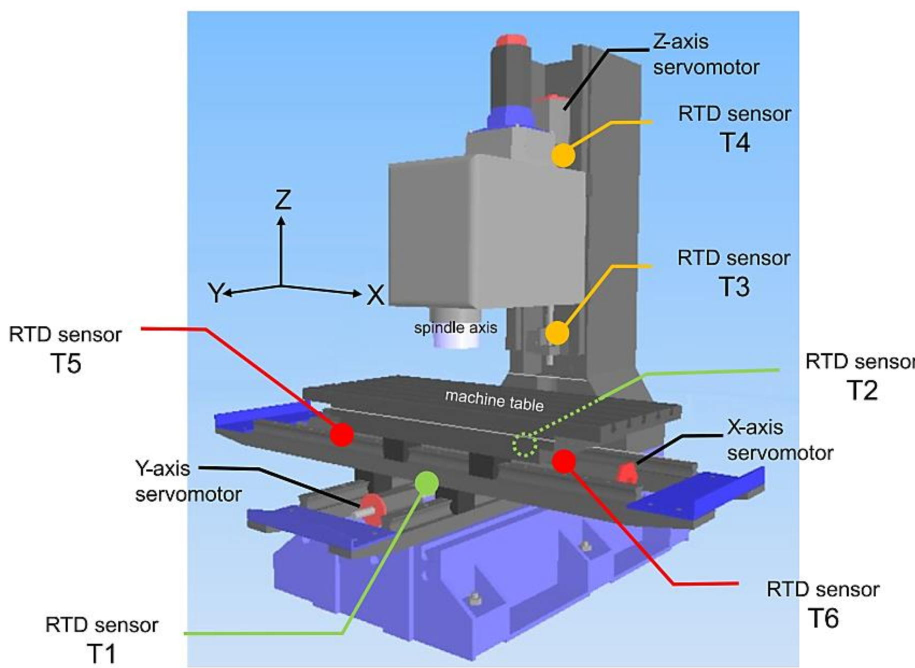

Fig. 1 Layout of RTD temperature sensors on the three-axis CNC machine tool

The thermal positioning error was determined by a laser interferometer system. To ensure high-precision displacement measurements during machine operation, the interferometer was aligned along the machine axis under study, as shown in Figure 2 [21]. Temperature measurements from the RTD sensors and displacement measurements from the laser interferometer were recorded simultaneously under different thermal operating conditions. The measured positioning error was then taken as the target variable for the development and validation of the proposed thermal error prediction model.

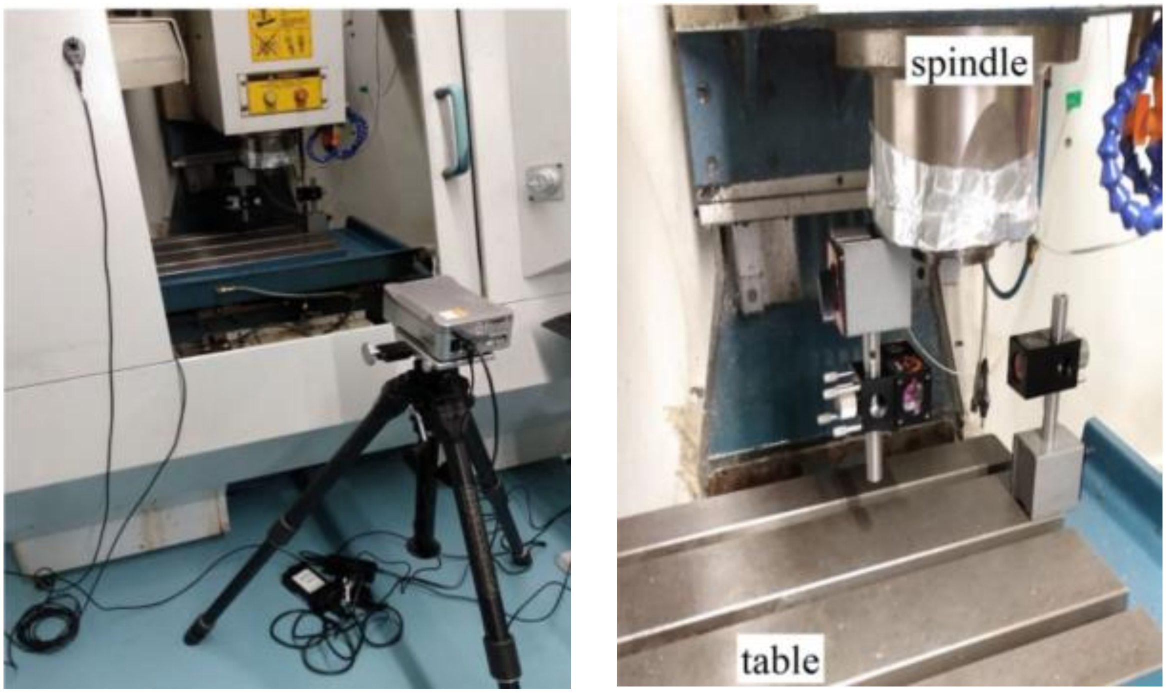

(a) (b)

Fig. 2 Laser interferometer setup for thermal positioning error measurement

2.2. Dataset Description

The dataset comprised temperature measurements collected by the RTD sensors and the thermal positioning error data. These data were subsequently used as input-output pairs for developing and validating the machine-learning-based thermal error prediction model. The Pearson correlation matrix between the input variables (X, Y, Z, DeltaTX5, DeltaTX6, DeltaTY1, DeltaTY2, DeltaTZ3, and DeltaTZ4) and the output variables (ErrX, ErrY, and ErrZ) is illustrated in Figure 3. Specifically, strong positive correlations were observed between X and ErrX (r = 0.93), Y and ErrY (r = 0.96), and Z and ErrZ (r = 0.86). The thermal variables are also highly correlated with each other, with a correlation coefficient of 0.97 between DeltaTX5 and DeltaTX6, indicating that both sensors respond to the same thermal changes within the X-axis subsystem.

Similarly, DeltaTY1 and DeltaTY2 (r = 0.83) as well as DeltaTZ3 and DeltaTZ4 (r = 0.77) exhibit strong positive correlations, indicating that these sensor pairs experience similar thermal dynamics. In addition, DeltaTX5 and DeltaTX6 are moderately to strongly negatively correlated with ErrX (r = -0.71 and -0.63, respectively) and DeltaTZ3 and DeltaTZ4 are negatively correlated with ErrZ (r = -0.68 and -0.51, respectively). The correlation patterns observed show that the thermal positioning error is affected by both position and temperature. Moreover, the high inter-variable correlation and the varying input-output relations indicate complex thermal interactions that cannot be well represented by simple linear models, thus providing the motivation for applying nonlinear machine-learning methods.

The spatial and statistical properties of the thermal positioning errors in the experimental dataset along the X-, Y-, and Z-axes are shown in Figure 4 and Figure 5, respectively. As illustrated in Figure 4, the normalized thermal errors exhibit distinct spatial distributions across the machine workspace, with each error component (ErrX, ErrY, and ErrZ) showing a unique variation pattern along the corresponding machine axis. These behaviors show high dependency of the thermal positioning error on the machine kinematic positions, and reflect the thermo-mechanical deformation mechanisms of the CNC machine structure. Spatial maps of the various colors also show a gradual change in color, indicating that the thermal deformations are not uniform across the workspace, meaning that there is a nonlinear relationship between the machine coordinates and the thermal errors.

As shown in the statistical distributions in Figure 5, all three thermal error components show significant positive skewness, with most of the samples being at relatively low levels of error and a small number of samples at relatively high levels of thermal error. This distribution pattern suggests that the machine is thermally stable for most of the working situations, and only a few regions of the workspace or some thermal states have large thermal errors. This imbalance creates additional challenges for model development from a machine learning point of view because prediction algorithms could become biased towards the dominant region of low error and have less sensitivity to rare but important large error events. The dataset thus reflects a realistic situation of industrial operation and is a stringent test of the predictive performance and generalizability of thermal error prediction models. The overall results of the combined spatial and statistical analysis show that the synthesized dataset retains the key thermo-mechanical features of the CNC machine and has adequate variability for the development of effective data-driven thermal error compensation strategies. The relationships between the thermal sensor temperature variations and the thermal positioning errors along the X-, Y- and Z-axes are shown in Figures 6-8. The results show that there are weak to moderate correlations between the individual thermal variables and the positioning errors, while there is a large amount of data dispersion in all the pairs of sensor and error. This behavior indicates that the generation of thermal errors is not only a function of the single temperature measurement, but also a function of the interaction of different thermal sources, thermo-mechanical deformation mechanisms and machine kinematic conditions.

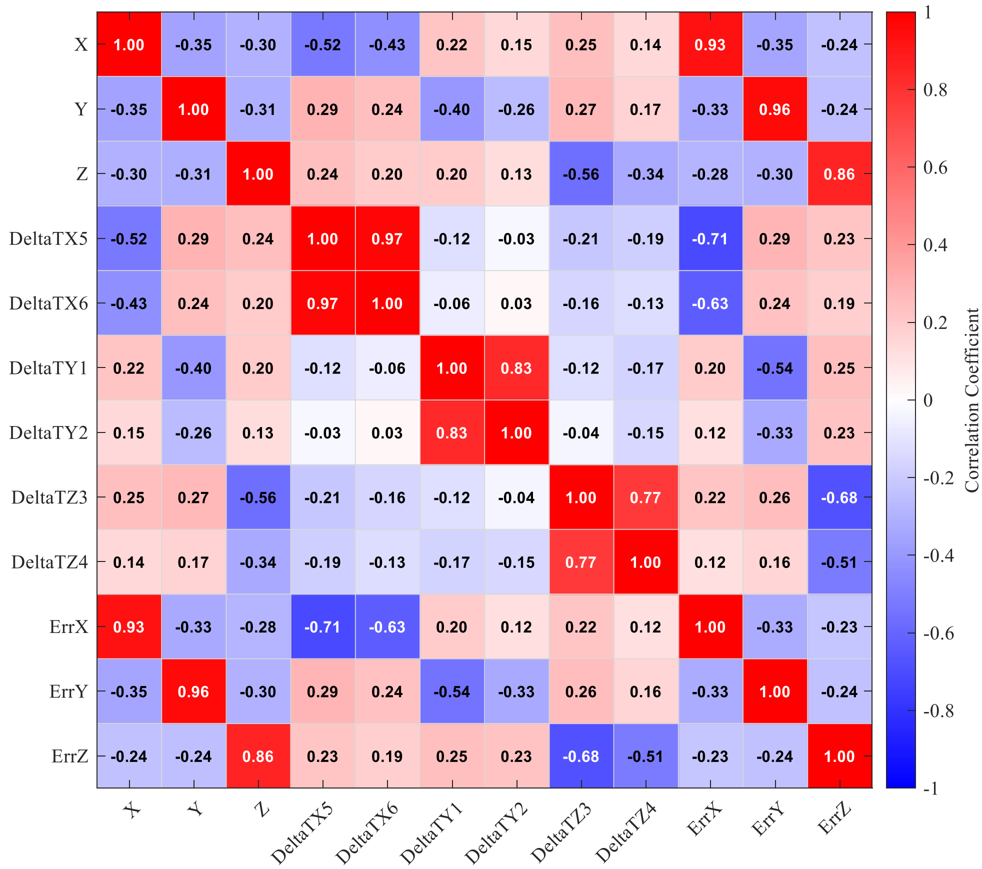

Fig. 3 Correlation analysis of machine coordinates, thermal sensor measurements, and thermal positioning errors in the CNC machine tool

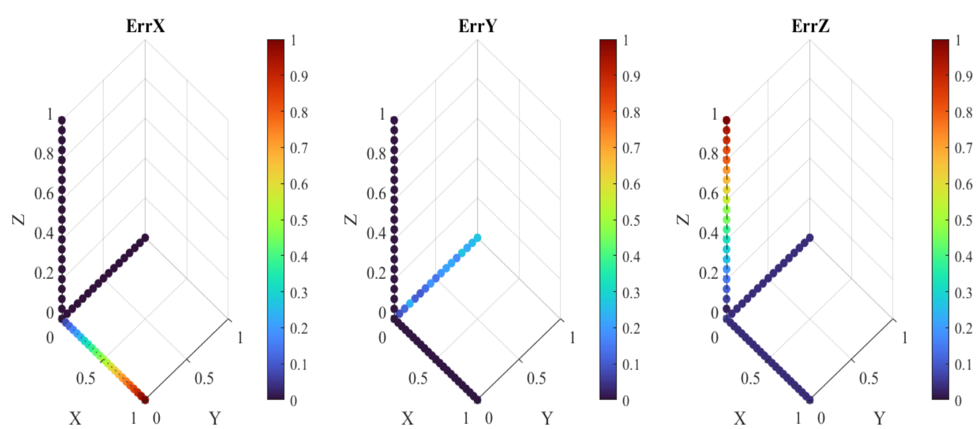

Fig. 4 Spatial distributions of normalized thermal errors (ErrX, ErrY, and ErrZ) in the synthesized dataset

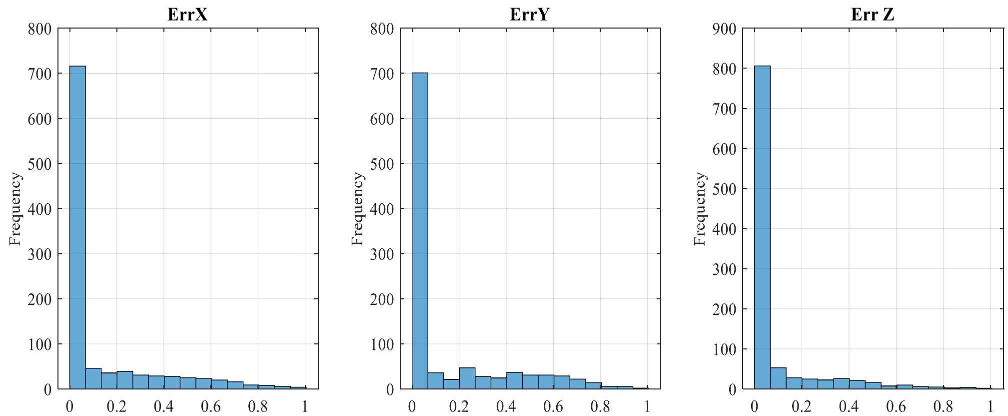

Fig. 5 Distribution of thermal positioning errors along the X-, Y-, and Z-axes

In addition, the wide variation in the points from the fitted trend lines suggests there are strong nonlinear relationships and coupling effects between the thermal and positional states. The variety of the thermal operating conditions of the samples further demonstrates the diversity and representativeness of the synthesized data. The outcomes are in line with the multidimensional, nonlinear nature of the thermal positioning errors, and support the application of complex machine learning models, such as artificial neural networks, for the prediction and compensation of thermal errors. The experimental dataset consisted of 1,036 samples, randomly split into two to develop and test the model. In particular, 70% of the data were used for training the model to learn the relationships between the input variables and the thermal positioning errors, and the remaining 30% were used for testing the model to evaluate its prediction performance and generalization ability. The data partitioning was done by using Monte Carlo random sampling to ensure that both the subsets were representative of the statistical properties of the entire dataset and to reduce sampling bias. This method improves the strength and stability of model evaluation by sampling training and testing data from the entire operating conditions and thermal states in the dataset.

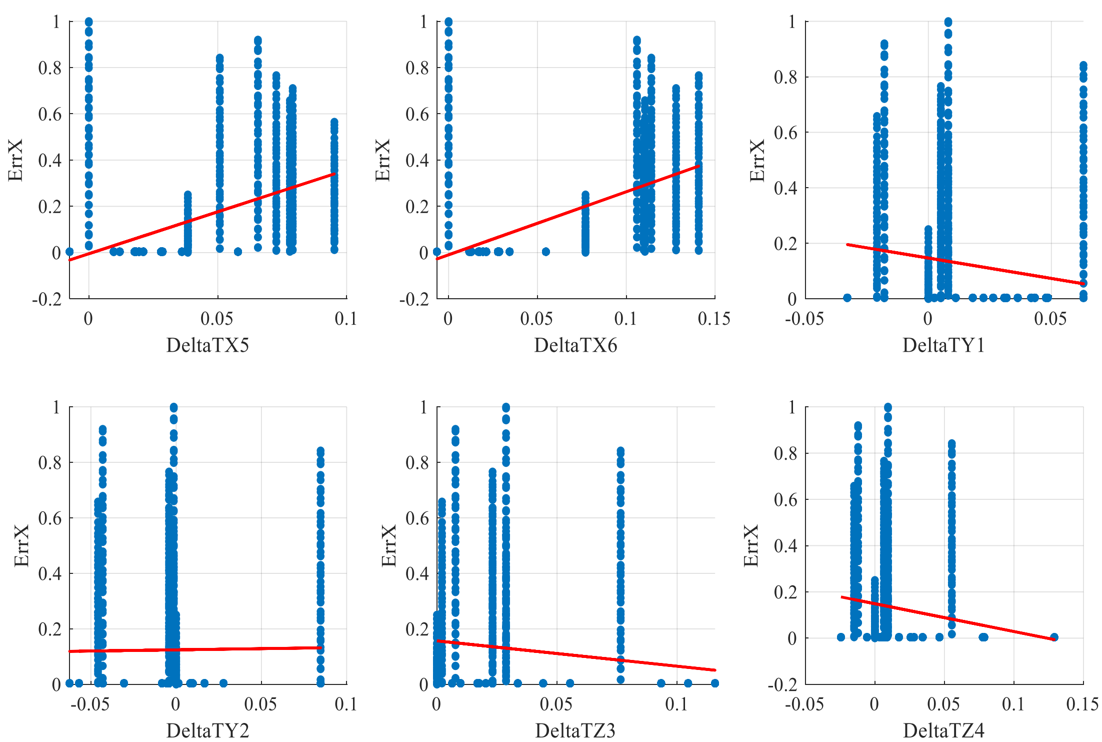

Fig. 6 Scatter distributions of thermal sensor temperature variations and thermal positioning error along the X-axis (ErrX)

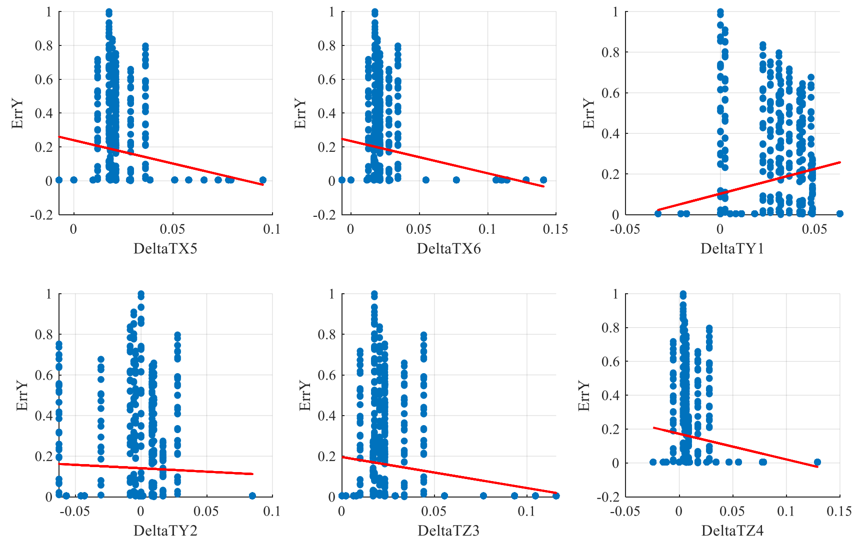

Fig. 7 Scatter distributions of thermal sensor temperature variations and thermal positioning error along the Y-axis (ErrY)

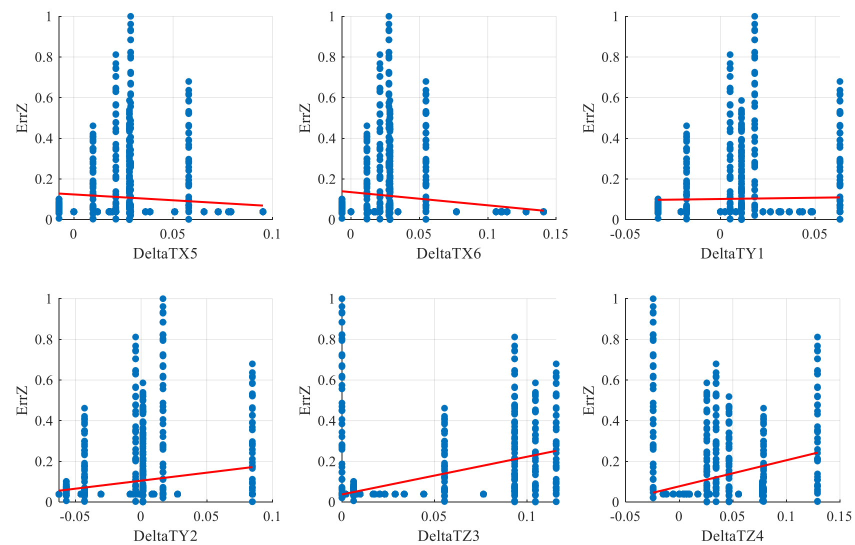

Fig. 8 Scatter distributions of thermal sensor temperature variations and thermal positioning error along the Z-axis (ErrZ)

2.3. Neuron-Optimized Artificial Neural Network (NO-ANN)

Figure 9 illustrates the overall workflow adopted for developing and validating the proposed NO-ANN framework, from raw thermal error data acquisition to final statistical validation. Raw CNC thermal error data are first cleaned and normalized to a common scale before being partitioned into independent training and testing subsets. The training subset is used within a Monte Carlo-based hidden-neuron sweep, in which multiple network configurations are trained and repeatedly evaluated to compute a composite performance score. The optimal NO-ANN configuration is then identified as the architecture achieving the lowest composite score across all Monte Carlo repetitions. This selected model is subsequently evaluated on the independent testing subset to assess its final predictive performance. Statistical validation and benchmarking against established models are finally performed to confirm the robustness, generalization capability, and practical relevance of the proposed framework.

ANNs are well known for their universal approximation properties and powerful learning ability, and have been extensively used for modelling complex nonlinear systems [44]. Thermal deformation in CNC machine tools arises from multiple internal heat sources and the thermal interactions between machine components, which cause very nonlinear thermal positioning errors. Thus, ANN models are especially suitable for establishing the relationship between thermal-sensitive variables and thermal positioning errors.

In this research, a single hidden-layer feedforward ANN was developed for thermal error prediction of a three-axis CNC machine tool. The ANN architecture comprises nine input variables: the machine coordinates (X, Y, and Z) and the six thermal-sensitive temperature measurements (DeltaTX5, DeltaTX6, DeltaTY1, DeltaTY2, DeltaTZ3, and DeltaTZ4). The output layer consists of three neurons, representing the thermal positioning errors in the X, Y and Z directions, respectively, ErrX, ErrY and ErrZ.

The nonlinear mapping between the input variables and the predicted thermal positioning errors can be formulated as a network with n_h hidden neurons:

$$\hat{y}_k = g\left(\sum_{j=1}^{n_h} \vartheta_{jk}.\, f\left(\sum_1^9 w_{ij} x_i + b_j\right) + c_k\right) \qquad (1)$$

where x_i represents the i-th input variable, while w_{ij} and υ_{jk} are the synaptic weights connecting the input layer to the hidden layer and the hidden layer to the output layer, respectively, the terms b_j and c_k denote the bias coefficients of the hidden and output neurons. The hidden-layer transformation is governed by the activation function f(·), while the output response is determined by the activation function g(·). In this study, the hyperbolic tangent sigmoid (tansig) function was employed in the hidden layer for its bounded, smooth nonlinear response in modeling complex nonlinear thermal behaviors, while a linear activation function (purelin) was applied in the output layer to allow unrestricted, accurate prediction of continuous thermal positioning errors. The network topology was intentionally limited to a single-hidden-layer feedforward ANN, consistent with the Universal Approximation Theorem, which states that one hidden layer with a sufficient number of neurons can approximate any continuous nonlinear function. This choice allows the number of hidden neurons - the primary variable investigated in this study - to be optimized without introducing additional architectural degrees of freedom.

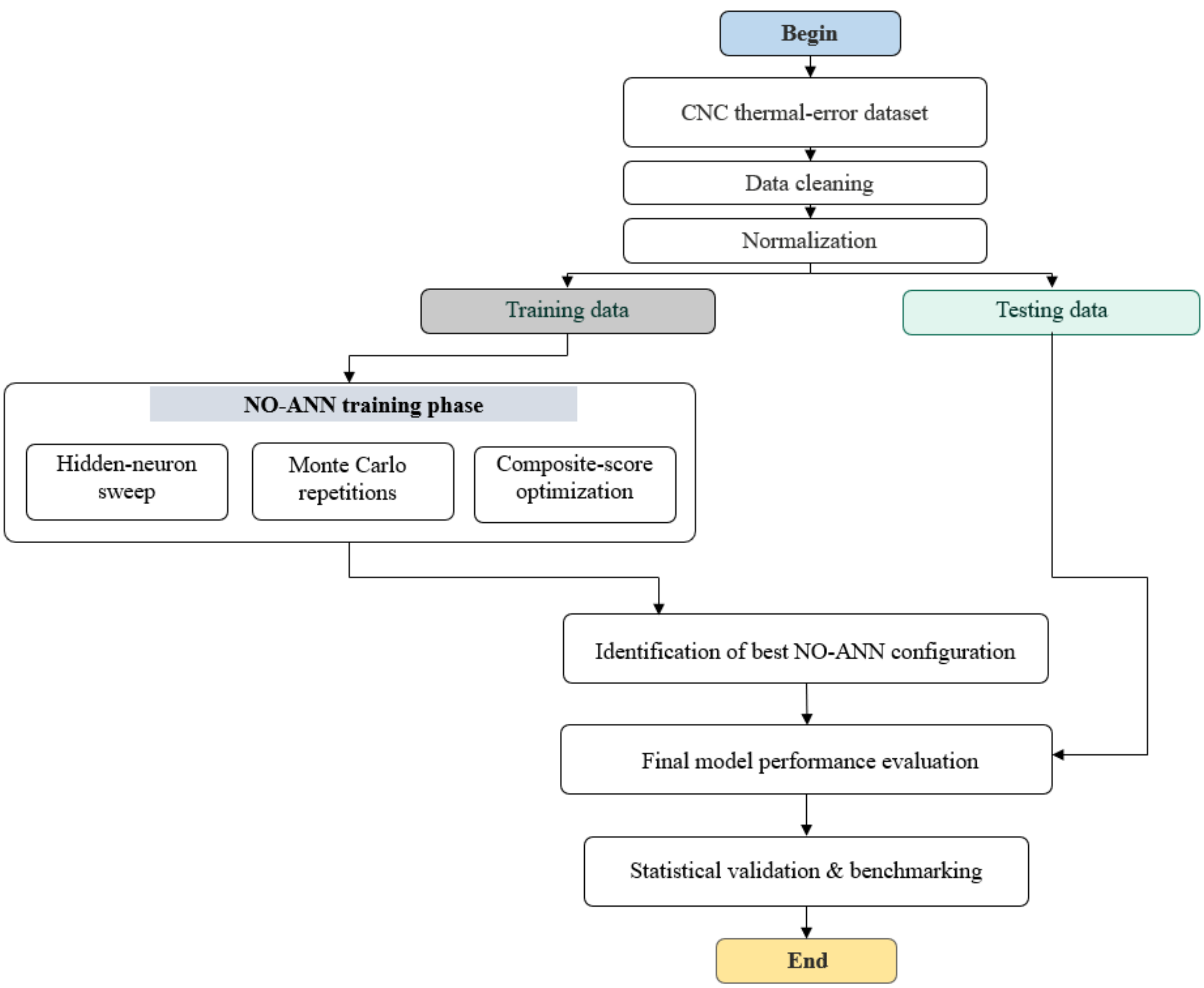

Fig. 9 Overall workflow of the proposed NO-ANN framework

The network parameters were trained using The Levenberg-Marquardt Backpropagation Algorithm (trainlm) in MATLAB (Neural Network Toolbox). All input and output variables were normalized to [0, 1] using min-max scaling prior to training. For each Monte Carlo repetition, the training and testing subsets were generated using a fixed random seed, and training was terminated when the maximum number of epochs (1000) or the mean-squared-error training goal (1×10^{-6}) was reached; no separate validation subset was used, as generalization was instead assessed through the independent test partition repeated over the 500 Monte Carlo trials. Overfitting was mitigated through early stopping, whereby training halted once the mean-squared-error goal or epoch limit was reached, preventing excessive fitting to training noise. A dedicated validation subset was not required because the Monte Carlo framework already supplied robustness evidence, evaluating each architecture on 500 independent, previously unseen test partitions. This repeated-resampling procedure is analogous to Monte Carlo cross-validation, since architecture selection relied on aggregated test-set performance across many random splits rather than a single training-testing partition.

The close agreement between training and testing metrics reported in Tables 1 and 2 further confirms that the selected architecture generalizes well rather than overfitting the training data.

The proposed model rests on two assumptions. First, the input-output mapping is treated as static, based on instantaneous coordinate and temperature readings rather than explicit time-history terms, which may reduce accuracy under transient thermal conditions. Second, training and testing samples are assumed to share a common statistical population, reflecting the same machine, sensor configuration, and operating range; reported performance, therefore, applies within this experimental domain.

The ability of the ANN model to predict was assessed by the Coefficient of Determination (R^2), Root Mean Square Error (RMSE) and Mean Absolute Error (MAE) [45]:

$$R^2 = 1 - \left[\frac{\sum_1^n (m_i - \widehat{m}_i)^2}{\sum_i^n (m_i - \overline{m})^2}\right] \tag{2}$$

$$MAE = \frac{1}{n}\sum_1^n |m_i - \widehat{m}_i| \tag{3}$$

$$RMSE = \sqrt{\frac{1}{n}\sum_1^n (m_i - \widehat{m}_i)^2} \tag{4}$$

where n denotes the total number of data samples, $\widehat{m}_i$ is the predicted value, $\overline{m}$ The mean of the actual values of the dependent variable, and m_i is the observed value.The number of hidden neurons is one of the most important factors that influence the performance of an ANN. The Universal Approximation Theorem states that a single hidden-layer feedforward neural network with enough hidden neurons can approximate any continuous nonlinear function. However, selecting an appropriate number of hidden neurons is critical, as too few neurons may cause underfitting, whereas too many neurons may lead to overfitting.

The number of hidden neurons was systematically varied from 1 to 30 to find the optimum hidden-neuron architecture. The ANN model was trained and tested 500 times for each configuration of the neurons using random partitions of training-testing data. Median values of RMSE, MAE and R^2 were then computed to evaluate the model predictive accuracy, and the Interquartile Range (IQR) of RMSE was computed to quantify the model stability and robustness.

A two-step optimization process was used to determine the optimal architecture of the hidden neurons. First, the effect of the hidden-neuron number on the prediction performance of ANNs was explored by calculating the median and interquartile range statistics of RMSE, MAE and R^2 from 500 Monte Carlo simulations.

Second, a composite score was introduced to simultaneously evaluate prediction accuracy, goodness-of-fit, and model stability. The composite score was defined as:

$$Score = \frac{RMSE_n + R^2_{inv,n} + IQR_{RMSE,n}}{3} \tag{5}$$

where $RMSE_n$, $R^2_{inv,n}$ and $IQR_{RMSE,n}$ denote the normalized values of RMSE, inverted coefficient of determination, and RMSE interquartile range, respectively.

All metrics were normalized into the interval [0,1] using min-max normalization:

$$X_n = \frac{X - X_{min}}{X_{max} - X_{min}} \tag{6}$$

Since larger R^2 values indicate better prediction performance, the normalized coefficient of determination was inverted according to:

$$R^2_{inv,n} = 1 - R^2_n \tag{7}$$

where:

$$R^2_n = \frac{R^2 - R^2_{min}}{R^2_{max} - R^2_{min}} \tag{8}$$

RMSE was chosen as the key error metric for the composite score, as RMSE and MAE had very similar trends for all hidden neuron configurations. Using both metrics would give too much weight to prediction error and too little to model robustness. Hence, the RMSE, R^2 and RMSE-IQR were used to balance the assessment of prediction accuracy, goodness-of-fit and model stability.

The hidden-neuron configuration yielding the lowest composite score was selected as the optimal network configuration. This approach provides a robust basis for identifying a model that achieves high predictive accuracy while maintaining good stability and generalization performance for thermal error prediction in CNC machine tools.

3. Results and Discussion

3.1. Determination of the Optimal ANN Architecture

As shown in Figure 10(a), the median RMSE values of both the training and testing datasets decrease rapidly as the number of hidden neurons is increased from 1 to about 8 neurons, which demonstrates a significant improvement in the ability of the ANN to model the nonlinear relationship between the thermal-sensitive variables and thermal positioning errors. Beyond this point, the RMSE curves level off and only minor gains are seen with additional network complexity. The same behavior is seen in the MAE in Figure 10(b), where the prediction error drops quickly at low numbers of neurons and then settles down to a close value. Correspondingly, the Coefficient of Determination (R^2) rises sharply from around 0.43 to values close to 1 and then stays almost constant with the addition of more hidden neurons, as seen in Figure 10(c). The close agreement between the two datasets suggests that the ANN has a good generalization capability and has not shown much overfitting even with the use of a relatively high number of hidden neurons. In addition, the small error bars around the Interquartile Range (IQR) indicate that the prediction performance is not significantly affected by random initialization and data partitioning, which highlights the robustness of the Monte Carlo evaluation framework.

As shown in Figure 11, the ANN architecture containing 11 hidden neurons achieved the lowest composite score (0.00215), followed by the architectures with 12 and 13 hidden neurons. Several nearby configurations predicted the data with similar accuracy, but the 11-neuron configuration had the best accuracy, goodness-of-fit, and robustness. Specifically, this architecture had a median RMSE of 1.5983, a median (R^2) of 0.9971 and the lowest RMSE-IQR of the top-ranked architectures. The results show that adding more hidden neurons than 11 does not significantly improve the performance of the model, so there is no need to add more neurons to the model. Therefore, the ANN model with 11 hidden neurons was chosen as the best model for thermal error prediction. This architecture provides a favorable balance between prediction accuracy, robustness, and computational efficiency while maintaining strong generalization performance for thermal error prediction.

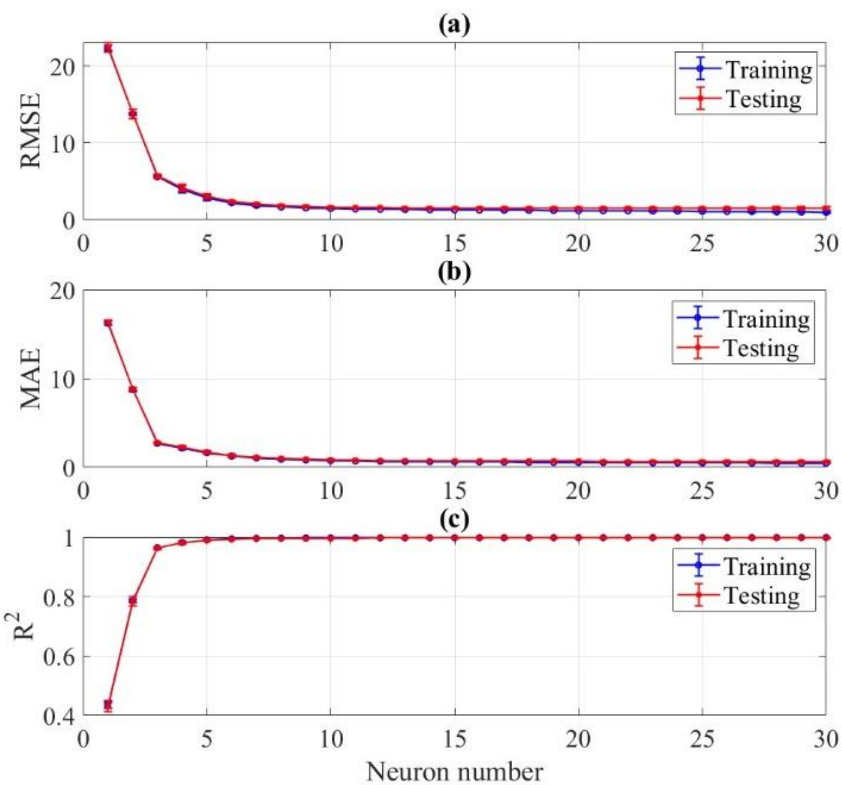

Fig. 10 Influence of hidden-neuron number on ANN prediction performance

========== TOP 10 NEURONS ==========

Neuron	RMSE_Median	R2_Median	RMSE_IQR	Score
11	1.5983	0.9971	0.11576	0.0021536
12	1.5737	0.99722	0.11822	0.0023797
13	1.5525	0.99726	0.12027	0.0025955
10	1.6525	0.99692	0.12666	0.0061677
14	1.5408	0.99733	0.14545	0.0093928
9	1.7151	0.99667	0.13503	0.0096467
15	1.5342	0.99732	0.1552	0.01201
17	1.5039	0.99742	0.16268	0.013562
16	1.5124	0.9974	0.17639	0.017528
8	1.8321	0.99618	0.16249	0.019455

Fig. 11 Top 10 hidden-neuron architectures ranked according to the composite performance score

3.2. Predictive Performance of the Optimal ANN Model

Following the hidden-neuron optimization process, the ANN architecture with 11 hidden neurons was selected as the optimal model and subsequently subjected to regression analysis.

Table 1. Axis-wise prediction performance of the optimized ANN model

Axis	Training dataset			Testing dataset		
	R^2	RMSE(μm)	MAE(μm)	R^2	RMSE(μm)	MAE(μm)
X-axis	0.9995	0.7864	0.4317	0.9994	0.7799	0.4469
Y-axis	0.9962	1.6491	0.8308	0.9947	2.023	1.0804
Z-axis	0.9981	1.2077	0.5923	0.9976	1.2870	0.6139

Table 2. Overall prediction performance of the optimized ANN model

Dataset	R^2	RMSE(μm)	MAE(μm)
Training dataset	0.9979	1.2144	0.6283
Testing dataset	0.9973	1.3633	0.7137
All data points	0.998	1.3247	0.6539

The prediction performance of the optimized ANN model for thermal positioning errors along X-, Y- and Z-axes is summarized in Table 1. The results demonstrate excellent predictive performance for all machine axes, with testing R^2 values exceeding 0.994 and prediction errors remaining at low levels. The similarity of the training and testing sets shows that the optimized ANN architecture has good generalization ability and is not seriously affected by overfitting. The prediction accuracy was best on the X-axis, with R^2, RMSE, and MAE values of 0.9994, 0.7799 μm, and 0.4469 μm, respectively, during the test. The Z-axis also showed very accurate predictions with an R^2 value of 0.9976 and an RMSE of 1.2870 μm in the test set. The prediction errors (RMSE = 2.023 μm and MAE = 1.0804 μm) were relatively large for the Y-axis, indicating that the thermal deformation behavior was more complex and the nonlinear interactions were stronger. However, the value of the corresponding testing (R^2) was still as high as 0.9947, indicating that the proposed ANN model was able to capture the dominant thermal error characteristics of the machine tool. The overall performance parameters reported in Table 2 further substantiate the effectiveness of the optimized ANN architecture. In particular, the model achieved R^2 values of 0.9979 and 0.9973 for the training and testing sets, respectively, and RMSE values of 1.2144 μm and 1.3633 μm, respectively. The slight gap between training and testing performance suggests that the predictive model is stable and robust, and has a good ability to generalize. Using the full dataset, the overall R^2 for the ANN model was 0.998, RMSE was 1.3247 μm, and MAE was 0.6539 μm, indicating excellent agreement between the ANN model prediction and the actual thermal positioning error.

The predictive capability of the optimized ANN model was further evaluated through regression analysis and direct comparison between measured and predicted thermal positioning errors, as presented in Figures 12 and Figure 13, respectively.

As illustrated in Figure 12, the thermal positioning errors of all three machine axes are confined to a narrow band around the ideal reference line (Y=T), with a good linear correlation between the ANN predictions and the experimental measurements. The fitted regression lines are very close to the reference line, indicating that the optimized ANN architecture can well represent the underlying nonlinear relationship between thermal-sensitive variables and thermal positioning errors and has a small systematic error. This is in line with the high prediction accuracy obtained for all axes ($R^2 > 0.994$ and RMSE < 2.1 μm). The predictive capability of the optimized ANN model was further validated using direct comparisons between measured and predicted thermal positioning errors, as shown in Figure 13. The thermal positioning errors are well predicted by the responses for the X-, Y-, and Z-axes over the entire operating range and their magnitudes and dynamic evolution are well captured. The ANN model well describes the progressive development, maximum values and cyclic variations of the thermal positioning errors under different thermal conditions. The measured values agree very well with the predicted values, and the general agreement is still good with slightly larger deviations at higher error levels, which demonstrates the ability of the model to represent complex thermal error behavior.

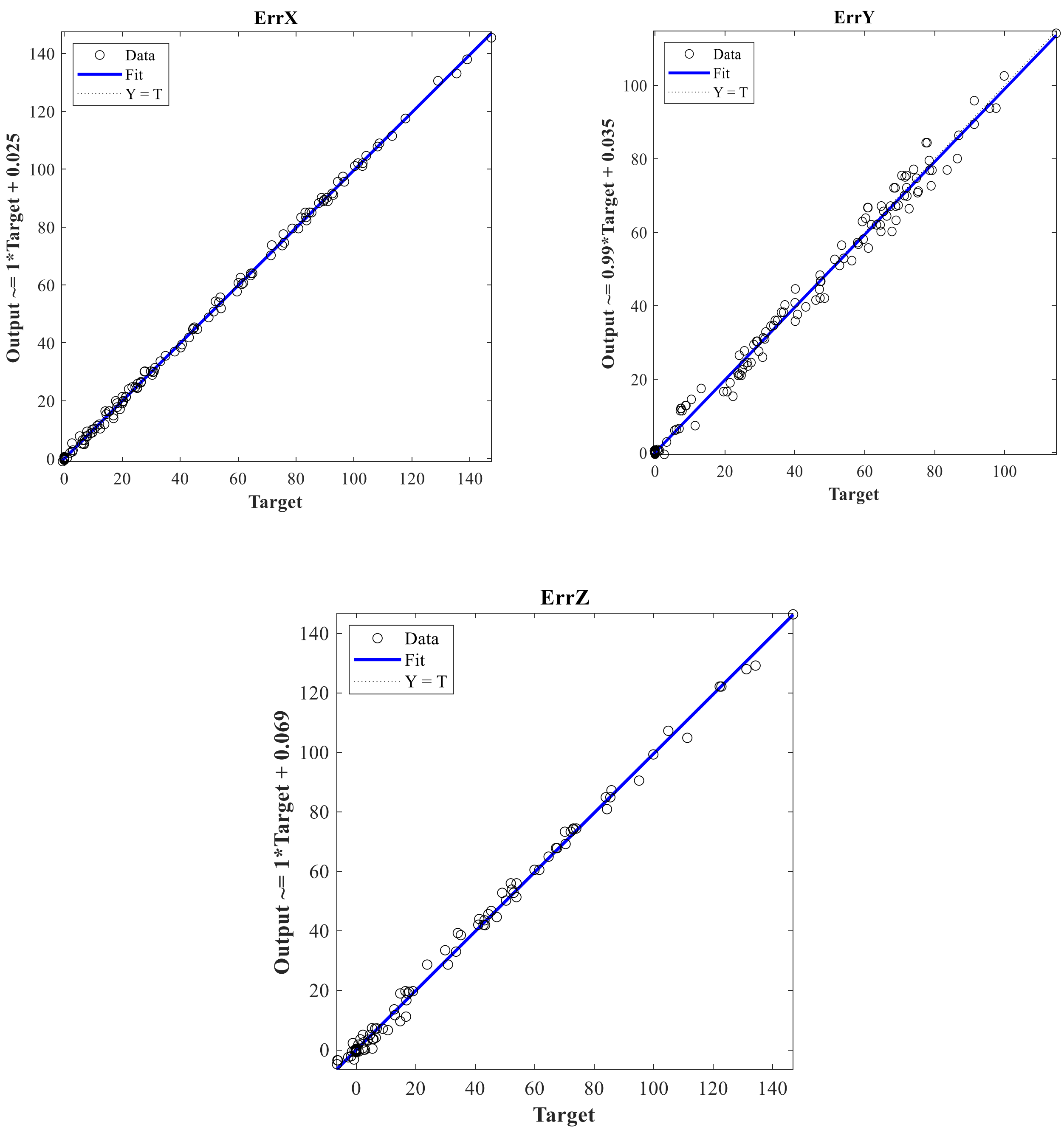

Fig. 12 Regression plots of the optimized ANN model for thermal positioning errors along the X-, Y-, and Z-axes

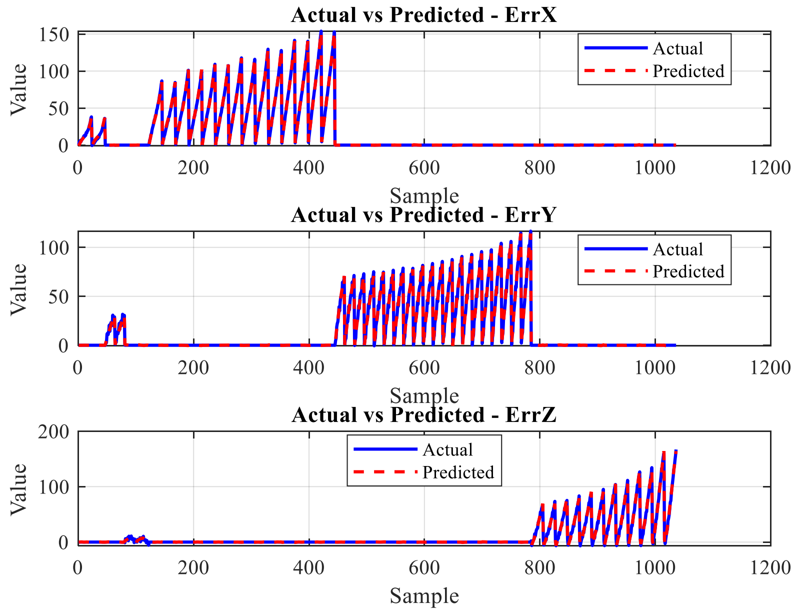

Fig. 13 Comparison between measured and predicted thermal positioning errors using the optimized ANN model

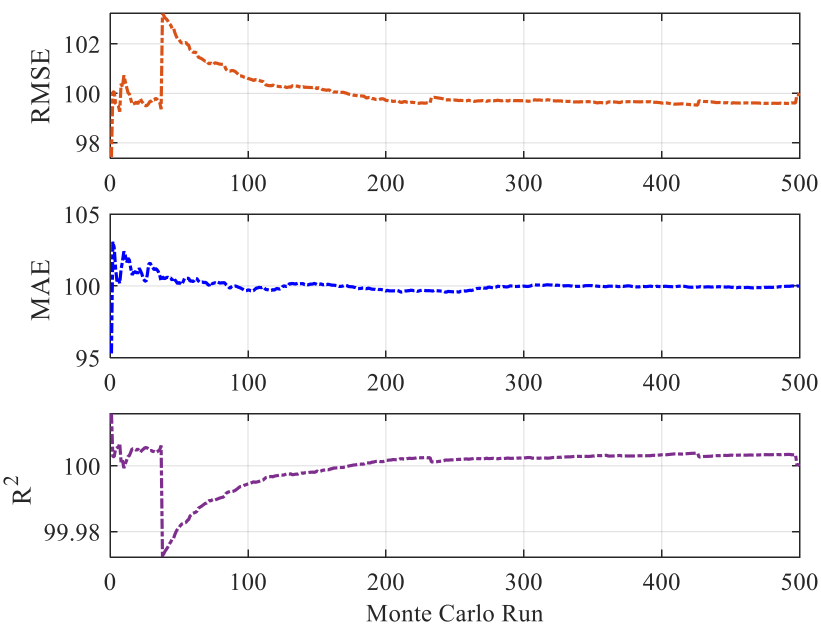

Fig. 14 Convergence of performance metrics for the optimized ANN architecture during Monte Carlo simulations

The convergence behavior of the ANN performance metrics over 500 Monte Carlo runs is presented in Figure 14. As can be seen from the RMSE, MAE and R^2 curves, there are relatively larger fluctuations in the first few runs, and then they converge as the number of runs increases. After about 200 Monte Carlo runs, the performance metrics are almost constant, and the variations in the estimates are relatively small, which means that the estimates are statistically stable enough. This finding indicates that the Monte Carlo framework adopted is able to consistently evaluate the performance and enhance the reliability of the hidden-neuron optimization process. The relative importance of the input variables used to estimate the thermal positioning errors in the X-, Y-, and Z-axes is shown in Figure 15. The results show that the three machine axes have different influence patterns, which means that the thermal error that is generated is influenced by different thermal and kinematic factors, depending on the direction of the motion.

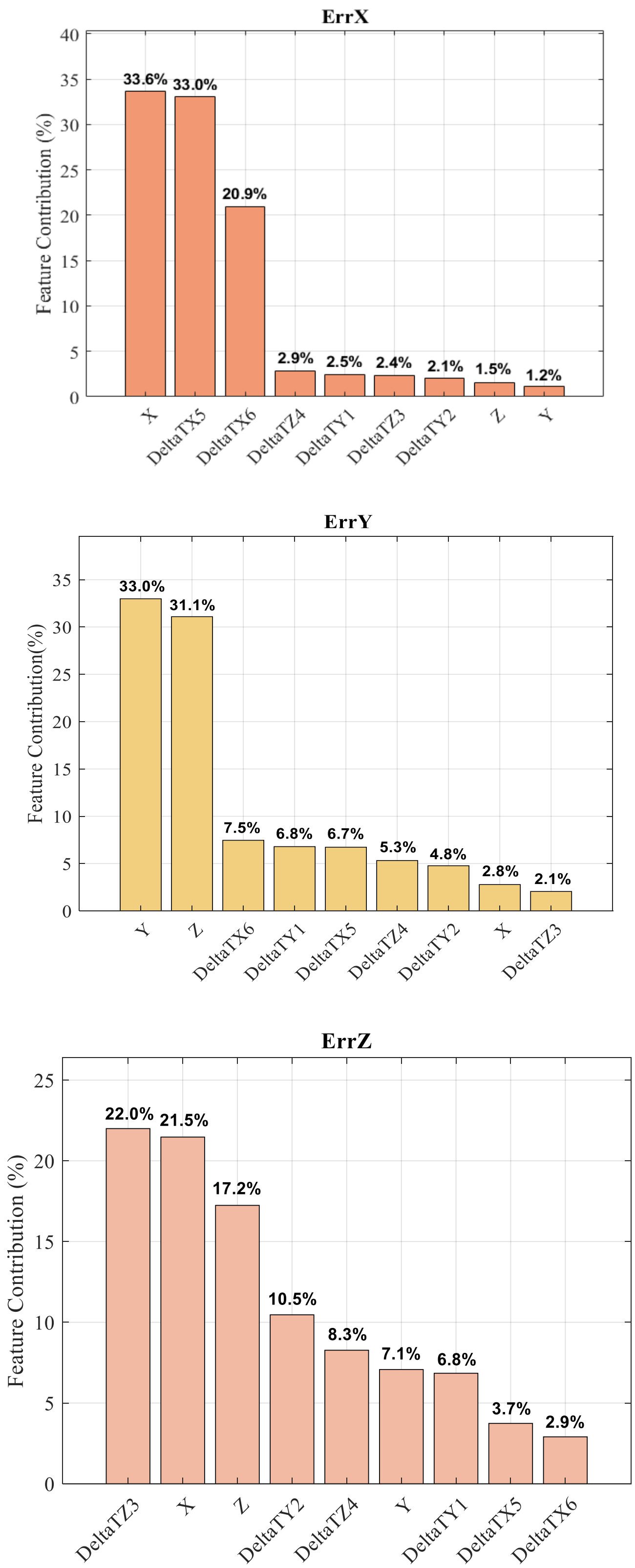

Fig. 15 Relative importance of input variables for thermal positioning error prediction along the X-, Y-, and Z-axes

To statistically validate the architecture selection, paired Wilcoxon signed-rank tests were performed on the RMSE test distributions across the 500 Monte Carlo repetitions, since identical training-testing partitions were used across neuron configurations at each repetition, enabling paired comparison. The selected 11-neuron architecture achieved significantly lower RMSE than the commonly used default of 10 neurons ($p = 9.7 \times 10^{-28}$) and than an under-parameterized 5-neuron network ($p = 9.1 \times 10^{-81}$). Although larger architectures (e.g., 20 neurons) achieved a marginally lower median RMSE ($p = 2.1 \times 10^{-18}$), Levene's test showed that their prediction variability was significantly higher ($p = 5.9 \times 10^{-5}$; IQR nearly doubled from 0.115 to 0.210 µm), confirming that the composite-score-based selection of 11 neurons provides the best trade-off between accuracy and stability rather than simply minimizing RMSE alone. A Friedman test across representative architectures (5, 8, 10, 11, 15, 20, 25 neurons) further confirmed that performance differences among configurations are statistically significant overall ($\chi^2 = 1803.6$, $p < 0.001$).

The main contributors to the X-axis error ErrX are the machine position X (33.6%), and the temperature measurements DeltaTX5 (33.0%) and DeltaTX6 (20.9%). In total, these variables account for about 87.5% of the predictive information, indicating that the thermal deformation along the X-axis is mainly related to the thermal status and positional dependence of the X-axis structure. All the other variables contribute relatively little and are not significant. The feature-importance distribution for ErrY differs substantially from that of ErrX. The two most important variables, Y and Z, are controlled by the machine with 33.0% and 31.1%, respectively. It indicates that the positioning error caused by the temperature in the Y-axis is greatly influenced by the position of the machine tool in the working space. The contribution pattern for temperature-related variables is more distributed than for the X-axis, suggesting that the thermal behavior of ErrY is due to several heat sources and interactions between structures. The most influential variables for the Z-axis error ErrZ are the temperature sensor DeltaTZ3 (22.0%), the machine coordinate Z (21.5%) and the coordinate X (17.2%). The distribution of the feature importance is more balanced when compared to the X- and Y-axis, which suggests that the thermal positioning error along the Z-axis is mainly controlled by a stronger coupling of thermal and geometric factors. The contributions of DeltaTY2, DeltaTZ4, Y and DeltaTY1 further support the existence of cross-axis thermal coupling effects in the machine structure.

3.3. Discussion

The prediction accuracy of different machine learning models used in previous studies for predicting the thermal error of CNC machine tools is summarized in Table 3. The results show that data-driven methods have been widely adopted to model the complex nonlinear relationship between thermal variations and machining errors. The traditional methods (such as multiple linear regression) typically had lower predictive ability, with reported RMSE values of approximately 2.79 µm and R^2 values less than 0.95. Advanced machine learning techniques, however, such as ANFIS, Gaussian Process Regression, GRU-Transformer, GWO-BiLSTM-SMOTE, and PSO-LSTM, showed better prediction accuracy as they were able to capture the nonlinear and dynamic thermal behavior. The proposed Neuron-Optimized Artificial Neural Network (NO-ANN) achieved an R^2 value of 0.998, RMSE of 1.3247 µm and MAE of 0.6539 µm, as shown in Table 3. These results are similar to or better than most of the models reported in the literature and summarized here. The results indicate that the optimization of hidden-layer neuron configuration can lead to a significant improvement in the predictive ability of ANN models with a relatively simple network structure. In addition to the selection of a learning algorithm, the selection of model architecture is also important in thermal error modeling, as it is evident in this observation. Note, however, that direct quantitative comparisons with other studies are not necessarily accurate as the performance metrics reported in the various studies are affected by a variety of factors such as machine tool type, sensor setup, thermal operating conditions, data type characteristics and validation methods. However, the comparative results suggest that the proposed NO-ANN model is a reliable and computationally efficient method for predicting the thermal error in CNC machine tools.

Unlike many previously reported studies that primarily introduce new algorithmic structures, such as LSTM, GRU-Transformer, or hybrid metaheuristic-optimized networks, to improve prediction accuracy, the present study addresses a complementary aspect of thermal error modeling. Specifically, it focuses on the systematic selection of hidden-layer architecture, which has received comparatively less attention in previous ANN-based thermal error prediction studies. Many reported ANN models determine the hidden-layer size empirically or through trial-and-error procedures without explicit quantitative selection criteria. The proposed NO-ANN framework introduces a systematic Monte Carlo-based optimization procedure using 500 repeated simulations. Prediction accuracy, goodness-of-fit, and model stability are evaluated using a composite performance score computed across repeated random weight initializations and stochastic training-testing partitions. Consequently, the selected architecture is supported by statistically aggregated evidence rather than the outcome of a single training run. This optimization strategy enables the selected ANN architecture to achieve a better balance between model complexity, prediction accuracy, and robustness. Rather than selecting the architecture that performs best in a single training run, the proposed framework identifies the configuration that consistently exhibits stable performance across repeated simulations. As a result, the optimized ANN reduces the influence of random initialization and data partitioning, thereby improving the reliability and generalization capability of thermal error prediction. This distinguishes the proposed framework from studies that primarily focus on developing new network architectures or optimizing network parameters through metaheuristic search strategies (Table 3). Therefore, the proposed framework provides an objective, statistically robust, and computationally efficient approach for hidden-layer architecture selection in ANN-based thermal error prediction of three-axis CNC machine tools.

Table 3. Performance comparison of thermal error prediction models for CNC machine tools

No.	Reference	Prediction model	Performance metrics
1	[10]	Bayesian neural network	$R^2 = 0.807$; RMSE = 1.998 μm; MAE = 1.741 μm
2	[34]	Adaptive Neuro-Fuzzy Inference System- Fuzzy C-Means (ANFIS-FCM)	$R^2 = 0.99$; RMSE = 2.78 μm
3	[46]	Gaussian Process Regression	$R^2 = 0.87882$; RMSE = 3.0922 μm; MSE = 9.5617 μm^2; MAE = 2.5841 μm
4	[47]	Multiple Linear Regression	$R^2 = 0.9454$; RMSE = 2.7914 μm; MAE = 2.2649 μm
5	[48]	Grey Neural Network Model with Convolution Integral (GNNMCI(1, N))	$R^2 = 0.98$; RMSE = 4.6 μm; E = 0.94 (higher efficiency coefficient)
6	[49]	Gated Recurrent Unit -Transformer (GRU-Transformer)	$R^2 = 0.9234$; MSE = 0.0388 μm^2; MAE = 0.1598 μm
7	[50]	Grey Wolf Optimizer - Bidirectional Long Short-Term Memory- Synthetic Minority Over-sampling Technique (GWO-BiLSTM-SMOTE)	$R^2 = 0.95384$ μm; RMSE = 1.09317 μm; MAE = 0.90654 μm
8	[51]	PSO-LSTM	MAE = 2.52 μm
9	[52]	SVM regression	RMSE = 0.03246 mm
10	Present work	Neuron-Optimized Artificial Neural Network (NO-ANN)	$R^2 = 0.998$; RMSE = 1.3247 μm; MAE = 0.6539 μm

3.4. Limitations and Future Work

Although the proposed NO-ANN framework achieves high predictive accuracy with a lightweight architecture of only 11 hidden neurons, several limitations should be acknowledged. First, real-time feasibility was not experimentally validated on a physical CNC controller in this study; however, the small network size means that forward inference requires only a few hundred floating-point operations per prediction, suggesting that real-time implementation is computationally feasible. This is consistent with recent studies that have successfully deployed lightweight neural-network-based thermal error compensation systems on physical CNC controllers in real time, achieving compensation rates exceeding 80% [53], and represents an important direction for future validation on the present platform. Second, the model assumes a static mapping between thermal-sensitive variables and positioning errors, calibrated for a fixed machine, sensor configuration, and operating range; sensor drift or recalibration over time could therefore degrade prediction accuracy, and periodic retraining or online adaptive updating would be required to maintain robustness during long-term industrial deployment. Third, the robustness of the model to sensor noise, faults, or partial sensor failure was not explicitly investigated and remains an open question. Future work will focus on experimental validation of real-time thermal error compensation on a physical CNC machine tool, development of online or adaptive retraining strategies to mitigate sensor drift, and extension of the proposed Monte Carlo-based hidden-neuron optimization framework to multi-axis and multi-machine configurations to further assess its scalability and generalization capability.

4. Conclusion

This study proposed a Neuron-Optimized Artificial Neural Network (NO-ANN) for predicting thermal positioning errors in a three-axis CNC machine tool. The optimization process resulted in an architecture of 11 hidden neurons with an overall prediction performance of $R^2 = 0.998$, RMSE = 1.3247 μm, and MAE = 0.6539 μm. The R^2 values of 0.9979 and 0.9973, and the RMSE values of 1.2144 μm and 1.3633 μm for training and testing, respectively, indicate the robustness and generalization ability of the developed model. The thermal-structural mechanisms that control thermal error generation were found to be different for each machine axis by feature importance analysis. The machine coordinates X and DeltaTX5, DeltaTX6 together contributed about 87.5% of the total predictive importance, which suggests that local thermal deformation plays a major role in the machine coordinate X. The machine coordinates Y (33.0%) and Z (31.1%) had a significant influence on ErrY, whereas the machine coordinates X and Z had negligible effects. This indicates that thermal errors are strongly dependent on the spatial position in the machining workspace. For ErrZ, the contributions of DeltaTZ3 (22.0%), Z (21.5%) and X (17.2%) are more balanced, indicating that there are significant thermal-geometric interactions and cross-axis thermal coupling effects. The proposed NO-ANN had competitive predictive performance with a relatively simple network structure, when compared to the previously reported thermal error prediction models. The results demonstrate that optimizing the hidden-neuron configuration can significantly improve the predictive performance of ANN models and provide a reliable basis for thermal error compensation in CNC machine tools.

Conflict of Interest

The authors declared no potential conflicts of interest with respect to the research, authorship, and/or publication of this article.

Data Availability Statement

The data that support the findings of this study are available on request from the corresponding author, to retain the privacy ethics of research. Also, most of the data is available within the article. The MATLAB code used for ANN training and Monte Carlo-based hidden-neuron optimization is available from the corresponding author upon reasonable request.

Funding Statement

No funding is provided for the preparation of the manuscript.

References

[1] Yu Wang et al., "A Review of the Application of Machine Learning Techniques in Thermal Error Compensation for CNC Machine Tools," *Measurement*, vol. 243, 2025. [CrossRef] [Google Scholar] [Publisher Link]

[2] Mohsen Soori, Behrooz Arezoo, and Roza Dastres, "Machine Learning and Artificial Intelligence in CNC Machine Tools, A Review," *Sustainable Manufacturing and Service Economics*, vol. 2, pp. 1-12, 2023. [CrossRef] [Google Scholar] [Publisher Link]

[3] Walid Chaaibi, Abderrazak El Ouafi, and Narges Omidi, "Geometric and Thermal-Induced Errors Prediction for Active Error Compensation in Machine Tools," *Journal of Experimental and Theoretical Analyses*, vol. 3, no. 4, pp. 1-19, 2025. [CrossRef] [Google Scholar] [Publisher Link]

[4] R Ramesh, M.A Mannan, and A.N Poo, "Error Compensation in Machine Tools - A Review: Part II: Thermal Errors," *International Journal of Machine Tools and Manufacture*, vol. 40, no. 9, pp. 1257-1284, 2000. [CrossRef] [Google Scholar] [Publisher Link]

[5] Josef Mayr et al., "Thermal Issues in Machine Tools," *CIRP Annals*, vol. 61, no. 2, pp. 771-791, 2012. [CrossRef] [Google Scholar] [Publisher Link]

[6] Yang Li et al., "A Review on Spindle Thermal Error Compensation in Machine Tools," *International Journal of Machine Tools and Manufacture*, vol. 95, pp. 20-38, 2015. [CrossRef] [Google Scholar] [Publisher Link]

[7] Zhiming Feng et al., "Study on Thermal Error Modeling for CNC Machine Tools based on the Improved Radial Basis Function Neural Network," *Applied Sciences*, vol. 13, no. 9, pp. 1-20, 2023. [CrossRef] [Google Scholar] [Publisher Link]

[8] Tao Cheng et al., "New Machining Test for Identifying Geometric and Thermal Errors of Rotary Axes for Five-Axis Machine Tools," *Measurement*, vol. 223, 2023. [CrossRef] [Google Scholar] [Publisher Link]

[9] Bo Huang et al., "Vertical Machining Center Feed Axis Thermal Error Compensation Strategy Research," *Applied Sciences*, vol. 13, no. 5, pp. 1-27, 2023. [CrossRef] [Google Scholar] [Publisher Link]

[10] Hu Shi et al., "Bayesian Neural Network–based Thermal Error Modeling of Feed Drive System of CNC Machine Tool," *International Journal of Advanced Manufacturing Technology*, vol. 108, pp. 3031-3044, 2020. [CrossRef] [Google Scholar] [Publisher Link]

[11] Hu Shi et al., "Investigation into Effect of Thermal Expansion on Thermally Induced Error of Ball Screw Feed Drive System of Precision Machine Tools," *International Journal of Machine Tools and Manufacture*, vol. 97, pp. 60-71, 2015. [CrossRef] [Google Scholar] [Publisher Link]

[12] Xinyuan Wei et al., "Thermal Error Modeling and Compensation based on Gaussian Process Regression for CNC Machine Tools," *Precision Engineering*, vol. 77, pp. 65-76, 2022. [CrossRef] [Google Scholar] [Publisher Link]

[13] Xiangfu Fu et al., "Digital Twin Technology in Modern Machining: A Comprehensive Review of Research on Machining Errors," *Journal of Manufacturing Systems*, vol. 79, pp. 134-161, 2025. [CrossRef] [Google Scholar] [Publisher Link]

[14] Wei Gao et al., "Machine Tool Calibration: Measurement, Modeling, and Compensation of Machine Tool Errors," *International Journal of Machine Tools and Manufacture*, vol. 187, 2023. [CrossRef] [Google Scholar] [Publisher Link]

[15] Guo-hua Chen et al., "Research on Thermal Error Compensation Modeling for the Machine Tool Integrated Drive System based on Energy Consumption Big Data and an Optimized Bidirectional Network," *Precision Engineering*, vol. 94, pp. 91-112, 2025. [CrossRef] [Google Scholar] [Publisher Link]

[16] T. Narendra Reddy et al., "Real-Time Thermal Error Compensation Strategy for Precision Machine Tools," *Materials Today: Proceedings*, vol. 22, no. 4, pp. 2386-2396, 2020. [CrossRef] [Google Scholar] [Publisher Link]

[17] Y.C. Liang et al., "Thermal Error Prediction for Heavy-Duty CNC Machines Enabled by Long Short-Term Memory Networks and Fog-Cloud Architecture," *Journal of Manufacturing Systems*, vol. 62, pp. 950-963, 2022. [CrossRef] [Google Scholar] [Publisher Link]

[18] Lisa Groos et al., "Mapping and Compensation of Geometric Errors of a Machine Tool at Different Constant Ambient Temperatures," *Precision Engineering*, vol. 63, pp. 10-17, 2020. [CrossRef] [Google Scholar] [Publisher Link]

[19] P. C. Tseng, and J. L. Ho, "A Study of High-Precision CNC Lathe Thermal Errors and Compensation," *International Journal of Advanced Manufacturing Technology*, vol. 19, pp. 850-858, 2002. [CrossRef] [Google Scholar] [Publisher Link]

[20] Srinivas N. Grama, Ashvarya Mathur, and Ashok N. Badhe, "A Model-based Cooling Strategy for Motorized Spindle to Reduce Thermal Errors," *International Journal of Machine Tools and Manufacture*, vol. 132, pp. 3-16, 2018. [CrossRef] [Google Scholar] [Publisher Link]

[21] Adalto de Farias, Marcelo Otávio dos Santos, and Ed Claudio Bordinassi, "Development of a Thermal Error Compensation System for a CNC Machine Using a Radial Basis Function Neural Network," *Journal of the Brazilian Society of Mechanical Sciences and Engineering*, vol. 44, 2022. [CrossRef] [Google Scholar] [Publisher Link]

[22] Otakar Horejš, Martin Mareš, and Lukáš Havlík, "Compensation of Thermally Induced Errors in Five-Axis Computer Numerical Control Machining Centers Equipped With Different Spindles," *Journal of Manufacturing Science and Engineering*, vol. 144, no. 10, pp. 1-10, 2022. [CrossRef] [Google Scholar] [Publisher Link]

[23] Hui Liu et al., "Thermal Error Modeling for Machine Tools: Mechanistic Analysis and Solution for the Pseudocorrelation of Temperature-Sensitive Points," *IEEE Access*, vol. 8, pp. 63497-63513, 2020. [CrossRef] [Google Scholar] [Publisher Link]

[24] Jialan Liu, Chi Ma, and Shilong Wang, "Data-Driven Thermally-Induced Error Compensation Method of High-Speed and Precision Five-Axis Machine Tools," *Mechanical Systems and Signal Processing*, vol. 138, 2020. [CrossRef] [Google Scholar] [Publisher Link]

[25] Martin Mareš, Otakar Horejš, and Lukáš Havlík, "Thermal Error Compensation of a 5-Axis Machine Tool Using Indigenous Temperature Sensors and CNC Integrated Python Code Validated With a Machined Test Piece," *Precision Engineering*, vol. 66, pp. 21-30, 2020. [CrossRef] [Google Scholar] [Publisher Link]

[26] Dang-Khoa Nguyen, Hua-Chih Huang, and Tzu-Chen Feng, "Prediction of Thermal Deformation and Real-Time Error Compensation of a CNC Milling Machine in Cutting Processes," *Machines*, vol. 11, no. 2, pp. 1-19, 2023. [CrossRef] [Google Scholar] [Publisher Link]

[27] Hong Yang, and Jun Ni, "Dynamic Neural Network Modeling for Nonlinear, Nonstationary Machine Tool Thermally Induced Error," *International Journal of Machine Tools and Manufacture*, vol. 45, no. 4, pp. 455-465, 2005. [CrossRef] [Google Scholar] [Publisher Link]

[28] Nico Zimmermann et al., "Adaptive Input Selection for Thermal Error Compensation Models," *CIRP Annals*, vol. 69, no. 1, pp. 485-488, 2020. [CrossRef] [Google Scholar] [Publisher Link]

[29] Nagesh Tambake et al., "Fault Diagnosis of a CNC Hobbing Cutter Through Machine Learning Using Three Axis Vibration Data," *Heliyon*, vol. 11, no. 2, pp. 1-28, 2025. [CrossRef] [Google Scholar] [Publisher Link]

[30] Z. Z. Xu et al., "Thermal Error Forecast and Performance Evaluation for an Air-Cooling Ball Screw System," *International Journal of Machine Tools and Manufacture*, vol. 51, no. 7, pp. 605-611, 2011. [CrossRef] [Google Scholar] [Publisher Link]

[31] Yu Chen, Yu Sun, and Wuxue Ding, "Thermo-Mechanical Coupling Model and Dynamical Characteristics of Press Actuator," *Procedia Engineering*, vol. 81, pp. 1657-1662, 2014. [CrossRef] [Google Scholar] [Publisher Link]

[32] Chengxin Zhang, Feng Gao, and Yan Li, "Thermal Error Characteristic Analysis and Modeling for Machine Tools Due to Time-Varying Environmental Temperature," *Precision Engineering*, vol. 47, pp. 231-238, 2017. [CrossRef] [Google Scholar] [Publisher Link]

[33] Hong Yang, and Jun Ni, "Dynamic Modeling for Machine Tool Thermal Error Compensation," *Journal of Manufacturing Science and Engineering*, vol. 125, no. 2, pp. 245-254, 2003. [CrossRef] [Google Scholar] [Publisher Link]

[34] Ali M. Abdulshahed, Andrew P. Longstaff, and Simon Fletcher, "The Application of ANFIS Prediction Models for Thermal Error Compensation on CNC Machine Tools," *Applied Soft Computing*, vol. 27, pp. 158-168, 2015. [CrossRef] [Google Scholar] [Publisher Link]

[35] Yang Li et al., "Thermal Error Modeling of Spindle based on the Principal Component Analysis Considering Temperature-Changing Process," *International Journal of Advanced Manufacturing Technology*, vol. 99, pp. 1341-1349, 2018. [CrossRef] [Google Scholar] [Publisher Link]

[36] Liang Ruijun et al., "The Thermal Error Optimization Models for CNC Machine Tools," *International Journal of Advanced Manufacturing Technology*, vol. 63, pp. 1167-1176, 2012. [CrossRef] [Google Scholar] [Publisher Link]

[37] Sen Mu et al., "A Review of Machine Learning-based Thermal Error Modeling Methods for CNC Machine Tools," *Machines*, vol. 13, no. 2, pp. 1-16, 2025. [CrossRef] [Google Scholar] [Publisher Link]

[38] Ying Gao, Xiaojun Xia, and Yinrui Guo, "A Modeling Method for Thermal Error Prediction of CNC Machine Equipment based on Sparrow Search Algorithm and Long Short-Term Memory Neural Network," *Sensors*, vol. 23, no. 7, pp. 1-26, 2023. [CrossRef] [Google Scholar] [Publisher Link]

[39] Jian Han et al., "Thermal Error Modeling and Compensation of a CNC Machining Center," *Advanced Materials Research*, vol. 490, pp. 1516-1520, 2012. [CrossRef] [Google Scholar] [Publisher Link]

[40] K. Gnana Sheela, and S.N. Deepa, "Review on Methods to Fix Number of Hidden Neurons in Neural Networks," *Mathematical Problems in Engineering*, vol. 2013, no. 1, pp. 1-11, 2013. [CrossRef] [Google Scholar] [Publisher Link]

[41] Huadong Li, Jingjun Liu, and Yang Li, "Research on Optimization of Temperature Sensitive Points of Machine Tool Thermal Error based on Independent Variable Selection Criteria," *Scientific Reports*, vol. 15, pp. 1-10, 2025. [CrossRef] [Google Scholar] [Publisher Link]

[42] Adalto Farias et al., "3-Axis Computer Numerical Control Machine Positioning Error Dataset for Thermal Error Compensation," *Data in Brief*, vol. 57, pp. 1-13, 2024. [CrossRef] [Google Scholar] [Publisher Link]

[43] Adalto Farias, and Ed Bordinassi, "Dataset for Thermal Error Compensation in a 3-Axis CNC Machine," *Mendeley Data*, vol. 1, 2024. [CrossRef] [Google Scholar] [Publisher Link]

[44] Nang Xuan Ho, Tien-Thinh Le, and Minh Vuong Le, "Development of Artificial Intelligence based Model for the Prediction of Young's Modulus of Polymer/Carbon-Nanotubes Composites," *Mechanics of Advanced Materials and Structures*, vol. 29, no. 27, pp. 5965-5978, 2022. [CrossRef] [Google Scholar] [Publisher Link]

[45] Yahao Chen et al., "Thermal Error Prediction Method of Transformer-GRU Composite Model for CNC Machine Tool Feeding System based on Multi-Source Information Fusion," *Measurement Science and Technology*, vol. 37, no. 7, 2026. [CrossRef] [Google Scholar] [Publisher Link]

[46] Wen-Lin Chu, "Integrating Machine Learning and Feature Analysis for Predicting and Managing Thermal Deformation in Machine Tools," *Case Studies in Thermal Engineering*, vol. 57, pp. 1-13, 2024. [CrossRef] [Google Scholar] [Publisher Link]

[47] Yu Li et al., "Thermal Error Analysis of Five-Axis Machine Tools based on Five-Point Test Method," *Lubricants*, vol. 10, no. 6, pp. 1-8, 2022. [CrossRef] [Google Scholar] [Publisher Link]

[48] Ali M. Abdulshahed et al., "Thermal Error Modelling of a Gantry-Type 5-Axis Machine Tool Using a Grey Neural Network Model," *Journal of Manufacturing Systems*, vol. 41, pp. 130-142, 2016. [CrossRef] [Google Scholar] [Publisher Link]

[49] Weimin Kang et al., "Thermal Error Modeling of Motorized Spindle Considering Temperature Hysteresis: A GRU-Transformer Prediction Model," *Case Studies in Thermal Engineering*, vol. 69, pp. 1-18, 2025. [CrossRef] [Google Scholar] [Publisher Link]

[50] Musab Alataiqeh et al., "Thermal Error Modeling of Slant Bed CNC Lathe Spindle based on BiLSTM With Data Augmentation and Grey Wolf Optimizer Algorithm," *Case Studies in Thermal Engineering*, vol. 70, pp. 1-18, 2025. [CrossRef] [Google Scholar] [Publisher Link]

[51] Xiangrui Zhao et al., "Research on Machine Tool Thermal Error Compensation based on an Optimized LSTM Model," *Actuators*, vol. 14, no. 12, pp. 1-26, 2025. [CrossRef] [Google Scholar] [Publisher Link]

[52] Van-Hai Nguyen et al., "Predicting Volumetric Error Compensation for Five-Axis Machine Tool Using Machine Learning," *International Journal of Computer Integrated Manufacturing*, vol. 36, no. 8, pp. 1191-1218, 2023. [CrossRef] [Google Scholar] [Publisher Link]

[53] Xingxing Yu et al., "Long-Term Thermal Error Modeling and Compensation for CNC Machine Tools based on Enhanced Autoformer," *International Journal of Advanced Manufacturing Technology*, vol. 140, pp. 3143-3158, 2025. [CrossRef] [Google Scholar] [Publisher Link]